Influence of Quantum Interference on the Thermoelectric Properties of Molecular Junctions

Ruijiao Miao[1], Hailiang Xu[2,3], Maxim Skripnik[4,5], Longji Cui[1], Kun Wang[1], Kim G. L. Pedersen[6,7], Martin Leijnse[2,8], Fabian Pauly[4,5], Kenneth Wärnmark[2,3], Edgar Meyhofer[1], Pramod Reddy[1,9*], and Heiner Linke[2,8*]*

[1] Department of Mechanical Engineering, University of Michigan, Ann Arbor, MI 48109, United States

[2] NanoLund, Lund University, Box 118, 22100 Lund, Sweden

[3] Department of Chemistry, Centre of Analysis and Synthesis, Lund University, Box 121, 22100 Lund, Sweden

[4] Okinawa Institute of Science and Technology Graduate University, Onna-son, Okinawa 904-0495, Japan

[5] Department of Physics, University of Konstanz, 78457 Konstanz, Germany

[6] Institute for Theory of Statistical Physics and JARA - Fundamentals of Future Information Technology, RWTH Aachen, 52056 Aachen, Germany

[7] Department of Chemistry, University of Copenhagen, 2100 Copenhagen, Denmark

[8] Solid State Physics, Lund University, Box 118, 22100 Lund, Sweden

[9] Department of Materials Science and Engineering, University of Michigan, Ann Arbor, MI 48109, United States

KEYWORDS: molecular junctions, thermoelectricity, quantum interference, thermopower

ABSTRACT: Quantum interference effects in molecular junctions have been proposed as an avenue for highly efficient thermoelectric power conversion at room temperature. Towards this goal, we investigated the effect of quantum interference on the thermoelectric properties of molecular junctions. Specifically, we employed oligo (phenylene ethynylene) (OPE) derivatives with a *para*-connected central phenyl ring (*para*-OPE3) and *meta*-connected central ring (*meta*-OPE3), which both covalently bind to gold via sulfur anchoring atoms located at their ends. In agreement with predictions from *ab-initio* modelling, our experiments on both single molecules and monolayers show that *meta*-OPE3 junctions, which are expected to exhibit destructive interference effects, yield a higher thermopower (with around 20 µV/K) compared to *para*-OPE3 (with around 10 µV/K). Our results show that

quantum interference effects can indeed be employed to enhance the thermoelectric properties of molecular junctions at room temperature.

Studies of the thermoelectric and electric properties of molecular junctions, created by bridging metallic electrodes by a single molecule or multiple molecules, not only reveal the fundamentals of charge transport through molecules, but also provide knowledge critical for developing molecule-based devices and their application in the field of energy conversion[1-6]. Recent computational studies have suggested that impressive thermoelectric performance, rivaling that of inorganic materials, can be obtained from molecular junctions by tuning their electronic transmission characteristics[7-13]. A particularly intriguing approach is to take advantage of quantum interference effects that arise in conjugated molecules[14-19], for example by using destructive interference to block low-energy electrons, while allowing high-energy electrons to pass[18]. In this way, one may approximate the ideal transmission function for thermoelectric power conversion at high efficiency[20]. A corresponding performance increase in molecules at room temperature has been predicted[18].

While past experimental work has probed the electric and thermoelectric properties of molecular junctions in both two terminal[7, 9-11,21-25] and three terminal[13] configurations, the effects of quantum interference on the thermoelectric performance have remained unexplored. In this letter we ask the question: Is it possible to introduce, in a predictable manner, quantum-interference effects in molecular junctions such that the experimentally observed thermoelectric properties are enhanced? We use the following approach: First, we introduce two specific molecules. While being isomerically similar, one of them is expected (based on modeling presented later) to show effects of destructive quantum interference, whereas the other one does not and can thus be used as a control. Subsequently, we will present our experimental results that indeed show a higher

thermoelectric voltage in the presence of quantum interference, which is in quantitative agreement with expectations from DFT-based modelling of coherent quantum transport.

The molecules we chose for our study are two OPE3 derivatives that feature different geometries at the central benzene ring (*para*- versus *meta*-connectivity, as shown in Figs. 1a and 1b). The choice of these two molecules is motivated by their expected different electron transmission characteristics. Specifically, the energy-dependent transmission in the gap between the highest occupied molecular orbital (HOMO) and the lowest unoccupied molecular orbital (LUMO) of *para*-connected junctions can be approximated by Lorentzians that are located at the HOMO and LUMO energies (Fig. 1c). *Meta*-connected junctions, on the other hand, are expected to feature a sharp antiresonance dip in their transmission characteristics in this range due to destructive quantum interference effects, as a consequence of the phase difference between the HOMO and LUMO transport channels of *meta*-OPE3 (see Fig. 1d)[26,27,28]. The resulting sharp feature in the transmission of *meta*-OPE3 is expected to lead to a larger Seebeck coefficient compared to *para*-OPE3 (see also computational results described below). The key question is now: Can this hypothesis regarding quantum-interference-related enhancement of the thermopower be experimentally confirmed?

To answer this question, we first measured the electrical conductance of OPE3-based single-molecule junctions using a break-junction technique that relies on a custom-built ultra-stable scanning tunneling microscope (STM)[29,30] (Fig. 1e). In these measurements, the OPE3-based molecules (whose synthesis is described in the Supporting Information (SI)) were first self-assembled onto a 7 mm × 7 mm sized template-stripped Au sample (150 nm thick), which was mounted into the STM. The STM tip was an electrochemically etched Au wire with a sharp tip, featuring a radius of around 30 nm.[31] In our experiments we first applied a 100 mV DC bias to the

tip, while the Au substrate with the self-assembled monolayer on it was grounded. Molecular junctions were formed by reducing the separation between the tip and the sample until they contacted each other, resulting in an electrical resistance of less than 1 kΩ. Subsequently, the Au tip was withdrawn from the Au substrate at a speed of 1.6 to 3.2 nm/s, during which molecules were stochastically trapped between the tip and the sample. The formation of molecular junctions was reflected through steps and plateaus in the electrical conductance traces, measured by monitoring the tunneling current through the junction at a sampling rate of 1 kHz. The inset of Fig. 2a shows representative conductance traces obtained in measurements of *para*-OPE3 junctions, where plateaus in the conductance frequently appear at around 10^{-4} G_0. In order to find the most probable conductance of the molecular junctions, we collected 2000 traces for *para*-OPE3 junctions and created histograms as shown in Fig. 2a. It can be seen that the most probable conductance (as obtained from the peak of the histogram) is $(1.2 \pm 0.6) \times 10^{-4}$ G_0 for Au-(*para*-OPE3)-Au junctions. Results from experiments and a similar analysis on Au-(*meta*-OPE3)-Au junctions are shown in Fig. 2b and reveal that their most probable electrical conductance is $(1.1 \pm 0.4) \times 10^{-5}$ G_0 – an order of magnitude smaller than those of the *para*-OPE3 junctions. This difference is consistent[28, 32] with the expected destructive interference in *meta*-OPE3 junctions (see Fig. 1d).

In order to measure the thermopower of single-molecule junctions, we created a stable temperature difference ($\Delta T \approx 0$, 15, 30 or 45 K) between the tip and sample by heating the sample holder via an integrated heater. The substrate temperature was monitored via a diode temperature sensor located on the sample holder. The tip was maintained at room temperature (around 295 K). When performing measurements at a given temperature differential ΔT, a single-molecule junction was created following the same approach employed in the electrical conductance measurements,

but with a reduced tip withdrawal speed of 0.2 nm/s. In order to perform thermoelectric measurements, the withdrawal of the tip was stopped when the electrical conductance reached the most probable conductance value as determined from the measurement data shown in Figs. 2a and 2b. Once the electrical conductance reached the desired value, we switched the bias applied to the tip with respect to the grounded sample from 100 mV to 0 V and monitored the thermocurrent I_{th} resulting from the applied ΔT via a current amplifier for a period of 100 to 500 ms. To confirm the integrity of the junction, we switched back to the 100 mV bias for 100 to 500 ms and checked if the electrical conductance was within a few percent of the most probable electrical conductance (see the SI for a detailed description of this process). If the conductance was not within a few percent of the most probable value, the experiment was terminated and the data from this measurement was discarded. This process of switching the bias from 100 mV to 0 V and back again to 100 mV was repeated until the single-molecule junction spontaneously broke. By performing many (on the order of several hundred) measurements like this we could collect the thermocurrent at each temperature differential $\Delta T = T_{substrate} - T_{tip}$. The obtained I_{th} is treated as positive, when the current flows from the tip (via the molecule) to the substrate, and negative, when it flows in the opposite direction. I_{th} was converted into a thermoelectric voltage ($\Delta V_{th} = V_{substrate} - V_{tip}$) by dividing -$I_{th}$ by G, that is, by the electrical conductance of the junctions before the withdrawal was stopped (see SI for a discussion of the sign of I_{th}). Histograms built from the thermoelectric voltage, collected at several temperature differentials, are shown in Fig. 2c for *para*-OPE3 junctions and in Fig. 2d for *meta*-OPE3 junctions. Similar measurements were also performed on benzenedithiol junctions, which have been studied in the past[7,30] and were repeated here as control experiments (shown in the SI). Finally, in Figs. 2e and 2f we present the

most probable thermoelectric voltages from the histograms as a function of the applied temperature differential. The thermopower of the molecular junction is given by:

$$S_{junc} = S_{Cu} - \Delta V_{th} / \Delta T \,, \tag{1}$$

where S_{Cu} = 1.94 μV/K is the Seebeck coefficient of bulk copper at T = 300 K (see the SI for details).

The Seebeck coefficients obtained from the thermopower slopes in Figs. 2e and 2f are 10.8 ± 9.5 μV/K and 20.9 ± 15.4 μV/K for the Au-(*para*-OPE3)-Au and Au-(*meta*-OPE3)-Au junctions, respectively. The positive sign in the Seebeck coefficient of OPE3-based junctions reveals that transport is hole-dominated. Remarkably, the thermopower of the Au-(*meta*-OPE3)-Au junction is twice as large as the thermopower of the Au-(*para*-OPE3)-Au junction. The data from single-molecule-junction Seebeck-coefficient measurements (shown in Figs. 2c-f) thus suggest that quantum interference effects can enhance thermoelectric properties. It should however be noted that there is a large spread in the thermoelectric voltages reported in Figs. 2c and 2d (as also reflected in Figs. 2e and 2f), possibly due to the intrinsic variability in the electronic structure of the junctions.

In order to ensure that our conclusions about the Seebeck coefficient are robust, we applied an approach developed by us in the past[22] that enables measurements of thermoelectric properties of junctions involving multiple molecules. These ensemble measurements are expected to present lower variability due to the averaging over junction geometries. In this method, the molecules were self-assembled onto Au substrates (see the SI for a characterization of monolayers). Subsequently, an Au-coated atomic force microscopy (AFM) probe was placed in gentle contact with the molecule-coated Au surface at a pushing contact force of around 1 nN (see Fig. 1f).

In order to measure the electrical conductance, the voltage bias across the molecular junction was varied from -0.5 V to 0.5 V and the current flowing through the junction (I) was measured. The measured I-V curves are shown in Figs. 3a,b and indicate that the low-bias conductances for Au-(*para*-OPE3)-Au junctions and Au-(*meta*-OPE3)-Au junctions are 3.8×10^{-2} G_0 and 1.9×10^{-3} G_0, respectively. The measured low-bias conductance is consistent with the expectation of roughly 100 molecules in the junction, when compared to the corresponding most probable single-molecule conductance.

Next, we determined the thermoelectric properties by varying the temperature differential ΔT from 0 to 3 K, while measuring I_{th} across the junction with the substrate grounded. The measured thermocurrent was converted into a thermoelectric voltage (similar to what was done in the single-molecule measurements, i.e. by dividing $-I_{th}$ by the electrical conductance), which is shown as a function of the applied temperature differential in Figs. 3c and 3d for Au-(*para*-OPE3)-Au and Au-(*meta*-OPE3)-Au junctions, respectively. Finally, using Eqn. 1 the Seebeck coefficient for the Au-(*para*-OPE3)-Au and Au-(*meta*-OPE3)-Au junctions is determined to be 8.0 ± 0.8 μV/K and 22.5 ± 1.1 μV/K respectively. The measured data confirm the conclusion from our single-molecule measurements that the Seebeck coefficient of *meta*-OPE3 junctions is over two times that of the *para*-OPE3 junctions.

To compare the measurements to theoretical expectation, we describe the electric and thermoelectric transport properties via the Landauer-Büttiker scattering theory of phase-coherent transport through nanostructures[2]. The central quantity in this approach is the energy-dependent transmission function $\tau(E)$. While we evaluate both the electrical conductance, G, and the thermopower, S_{junc}, exactly via energy integrals (see the SI for details), the following low-temperature expressions provide an excellent approximation:

$$G = G_0 \tau(E_F) \text{ and } S_{junc} = -\frac{\pi^2 k_B^2 T}{3e} \frac{d \ln \tau(E)}{dE}\bigg|_{E=E_F} . \quad (2)$$

In order to evaluate $\tau(E)$, we express the transmission in terms of Green's functions and use information on the electronic structure, as determined from density functional theory (DFT)[33]. These DFT calculations, which we also employ to determine stable contact geometries through energy optimization, were carried out with TURBOMOLE[34]. Since the actual energies of HOMO and LUMO levels with respect to the Fermi energy are crucial in the studied systems, we applied the DFT+Σ correction to overcome well-known shortcomings of DFT with regard to level alignments[35,36]. We have studied different contact geometries, where the sulfur anchoring atoms at both ends of the molecules bind either to a single or three gold atoms (see SI). The transmission curves for those junctions, where the sulfur atoms bind to three gold atoms, are shown in Fig. 4a. The antiresonance in the Au-(*meta*-OPE3)-Au junction is located around 1.3 eV above the Fermi energy E_F, while it is absent for Au-(*para*-OPE3)-Au. Following from the transmission at E_F, the calculated electrical conductance is 1.8×10^{-4} G_0 for Au-(*para*-OPE3)-Au and 3.85×10^{-6} G_0 for Au-(*meta*-OPE3)-Au. Compared to the experiment, these values differ by a factor of 1.8 and 0.32, respectively. Between *para* and *meta* configurations we see a significant difference in the derivatives $-d\ln\tau(E)/dE$ at the Fermi energy (Fig. 4b) and therefore in the Seebeck coefficients, which we find to be 7.31 µV/K for Au-(*para*-OPE3)-Au and 21.4 µV/K for Au-(*meta*-OPE3)-Au, respectively. The calculated Seebeck coefficients are thus within the experimental uncertainties. Our *ab-initio* modeling suggests that the doubling of the measured thermopower for Au-(*para*-OPE3)-Au junctions, in comparison to the Au-(*meta*-OPE3)-Au junctions, is due to the increased slope of the logarithm of the transmission function at E_F, as expected from destructive quantum interference effects.

In conclusion both our single-molecule and ensemble measurements revealed a larger thermopower for the Au-(*meta*-OPE3)-Au junctions as compared to Au-(*para*-OPE3)-Au junctions. Our measurements are in good agreement with theoretical *ab-initio* calculations (see Fig. 4), which predict such a difference as a result of quantum interference effects. Our results demonstrate that it is possible to use quantum interference phenomena to achieve an enhanced thermoelectric performance in molecular junctions at room temperature, opening a path towards quantum engineering of thermoelectric materials. In contrast, similar enhancement effects in semiconductor systems, e.g. in quantum dots[37], require cryogenic temperatures and are therefore not suitable for many purposes. Future thermoelectric applications of molecule-based devices require a larger power factor, that is, a large S_{junc} combined with a large G. This desirable combination has been predicted for specific molecules with a quantum-tailored transmission spectrum such as zinc-porphines[18], which will be the subject of future work.

ASSOCIATED CONTENT

Supporting Information.

Detailed information on experimental procedures, chemical synthesis protocols, characterization and computational methods.

AUTHOR INFORMATION

Corresponding Authors

*E-mail (Edgar Meyhofer): meyhofer@umich.edu

*E-mail (Pramod Reddy): pramodr@umich.edu

* E-mail (Heiner Linke): heiner.linke@ftf.lth.se

Author Contributions

The project was conceived by E.M., P.R., and H.L.. H.X. synthesized the molecules under the guidance of K.Wä.. R.M., L.C. and K.Wa. performed the experiments under the guidance of E.M. and P.R.. Calculations were performed by K.G.L.P. under the guidance of M.L and M.S. under the guidance of F.P.. The manuscript was written by R.M., P.R., and H.L. with contributions from all authors. All authors approved the final version of the manuscript.

Notes

The authors declare no competing financial interest.

ACKNOWLEDGMENT

P.R. and E.M. acknowledge funding from the Office of Naval Research (N00014-16-1-2672, instrumentation), the Department of Energy (DE-SC0004871, scanning probe microscopy). H.X. acknowledges financial support from the People Programme (Marie Curie Actions) of the European Union's Seventh Framework Programme (FP7-People-2013-ITN) under REA grant agreement n°608153 (PhD4Energy). H.L. acknowledges support by NanoLund, by the Royal Physiographical Society, by the Swedish Energy Agency (project P38331-1), by the Swedish Research Council (projects 621-2012-5122, 2014-5490), and by the Knut and Alice Wallenberg Foundation (project 2016.0089). M.L. acknowledges support by NanoLund and by the Swedish Research Council. We acknowledge the Lurie Nanofabrication Facility and Michigan Center for Material Characterization for facilitating the fabrication and calibration of devices. F.P. and M.S. acknowledge financial support by the Collaborative Research Center (SFB) 767 of the German Research Foundation (DFG). A large part of the numerical modelling has been carried out on computational resources provided by the state of Baden-Württemberg through the bwHPC initiative and the DFG through grant no INST 40/467-1 FUGG.

REFERENCES

1. Aradhya, S. V.; Venkataraman, L. *Nat Nanotechnol* **2013,** 8 (6), 399-410.
2. Cuevas, J. C.; Scheer, E., *Molecular electronics: an introduction to theory and experiment*. World Scientific: Singapore; Hackensack, NJ, 2010.
3. Cui, L.; Miao, R.; Jiang, C.; Meyhofer, E.; Reddy, P. *J Chem Phys* **2017,** 146 (9), 092201.
4. Song, H.; Reed, M. A.; Lee, T. *Adv Mater* **2011,** 23 (14), 1583-1608.
5. Lee, W.; Kim, K.; Jeong, W.; Zotti, L. A.; Pauly, F.; Cuevas, J. C.; Reddy, P. *Nature* **2013,** 498 (7453), 209-213.
6. Nitzan, A.; Ratner, M. A. *Science* **2003,** 300 (5624), 1384-1389.
7. Reddy, P.; Jang, S. Y.; Segalman, R. A.; Majumdar, A. *Science* **2007,** 315 (5818), 1568-1571.
8. Guo, S. Y.; Zhou, G.; Tao, N. J. *Nano Lett* **2013,** 13 (9), 4326-4332.
9. Widawsky, J. R.; Darancet, P.; Neaton, J. B.; Venkataraman, L. *Nano Lett* **2012,** 12 (1), 354-358.
10. Evangeli, C.; Gillemot, K.; Leary, E.; Gonzalez, M. T.; Rubio-Bollinger, G.; Lambert, C. J.; Agrait, N. *Nano Lett* **2013,** 13 (5), 2141-2145.
11. Rincon-Garcia, L.; Ismael, A. K.; Evangeli, C.; Grace, I.; Rubio-Bollinger, G.; Porfyrakis, K.; Agrait, N.; Lambert, C. J. *Nat Mater* **2016,** 15 (3), 289-294.
12. Tsutsui, M.; Morikawa, T.; He, Y. H.; Arima, A.; Taniguchi, M. *Sci Rep* **2015,** 5, 11519
13. Kim, Y.; Jeong, W.; Kim, K.; Lee, W.; Reddy, P. *Nat Nanotechnol* **2014,** 9 (11), 881-885.
14. Arroyo, C. R.; Tarkuc, S.; Frisenda, R.; Seldenthuis, J. S.; Woerde, C. H. M.; Eelkema, R.; Grozema, F. C.; van der Zant, H. S. J. *Angew Chem Int Ed* **2013,** 52 (11), 3152-3155.
15. Kaliginedi, V.; Moreno-Garcia, P.; Valkenier, H.; Hong, W. J.; Garcia-Suarez, V. M.; Buiter, P.; Otten, J. L. H.; Hummelen, J. C.; Lambert, C. J.; Wandlowski, T. *J Am Chem Soc* **2012,** 134 (11), 5262-5275.
16. Lambert, C. J. *Chem Soc Rev* **2015,** 44 (4), 875-888.
17. Finch, C. M.; Garcia-Suarez, V. M.; Lambert, C. J. *Phys Rev B* **2009,** 79 (3), 033405.
18. Karlström, O.; Linke, H.; Karlström, G.; Wacker, A. *Phys Rev B* **2011,** 84 (11), 113415.
19. Bergfield, J. P.; Solis, M. A.; Stafford, C. A. *ACS Nano* **2010,** 4 (9), 5314-5320.
20. Nakpathomkun, N.; Xu, H. Q.; Linke, H. *Phys Rev B* **2010,** 82 (23), 235428.
21. Baheti, K.; Malen, J. A.; Doak, P.; Reddy, P.; Jang, S. Y.; Tilley, T. D.; Majumdar, A.; Segalman, R. A. *Nano Lett* **2008,** 8 (2), 715-719.
22. Tan, A.; Balachandran, J.; Sadat, S.; Gavini, V.; Dunietz, B. D.; Jang, S. Y.; Reddy, P. *J Am Chem Soc* **2011,** 133 (23), 8838-8841.
23. Tan, A.; Sadat, S.; Reddy, P. *Appl Phys Lett* **2010,** 96 (1), 013110.
24. Tan, A. R.; Balachandran, J.; Dunietz, B. D.; Jang, S. Y.; Gavini, V.; Reddy, P. *Appl Phys Lett* **2012,** 101 (24), 243107.
25. Cui, L.; Miao, R.; Wang, K.; Thompson, D.; Zotti, L. A.; Cuevas, J. C.; Meyhofer, E.; Reddy, P. *Nat Nanotechnol* **2018,** 13 (2), 122-128.
26. Pedersen, K. G. L.; Strange, M.; Leijnse, M.; Hedegard, P.; Solomon, G. C.; Paaske, J. *Phys Rev B* **2014,** 90 (12), 125413.
27. Yoshizawa, K.; Tada, T.; Staykov, A. *J Am Chem Soc* **2008,** 130 (29), 9406-9413.
28. Manrique, D. Z.; Huang, C.; Baghernejad, M.; Zhao, X. T.; Al-Owaedi, O. A.; Sadeghi, H.; Kaliginedi, V.; Hong, W. J.; Gulcur, M.; Wandlowski, T.; Bryce, M. R.; Lambert, C. J. *Nat Commun* **2015,** 6, 6389.

29. Lee, W.; Reddy, P. *Nanotechnology* **2011,** 22 (48), 485703.
30. Kim, Y.; Lenert, A.; Meyhofer, E.; Reddy, P. *Appl Phys Lett* **2016,** 109 (3), 033102.
31. Huh, T. W.; Han, G.; Ban, W. J.; Ahn, H. S. *Int J Precis Eng Man* **2017,** 18 (2), 221-226.
32. Frisenda, R.; Tarkuc, S.; Galan, E.; Perrin, M. L.; Eelkema, R.; Grozema, F. C.; van der Zant, H. S. J. *Beilstein J Nanotech* **2015,** 6, 1558-1567.
33. Pauly, F.; Viljas, J. K.; Huniar, U.; Häfner, M.; Wohlthat, S.; Bürkle, M.; Cuevas, J. C.; Schön, G. *New J Phys* **2008,** 10, 125019.
34. *TURBOMOLE V7.2 2017* http://www.turbomole.com.
35. Zotti, L. A.; Bürkle, M.; Pauly, F.; Lee, W.; Kim, K.; Jeong, W.; Asai, Y.; Reddy, P.; Cuevas, J. C. *New J Phys* **2014,** 16, 015004.
36. Quek, S. Y.; Venkataraman, L.; Choi, H. J.; Louie, S. G.; Hybertsen, M. S.; Neaton, J. B. *Nano Lett* **2007**, 7 (11), 3477-3482.
37. Josefsson, M.; Svilans, A.; Burke, A. M.; Hoffmann, E. A.; Fahlvik, S.; Thelander, C.; Leijnse, M.; Linke, H. *arXiv:1710.00742 [cond-mat.mes-hall]*.

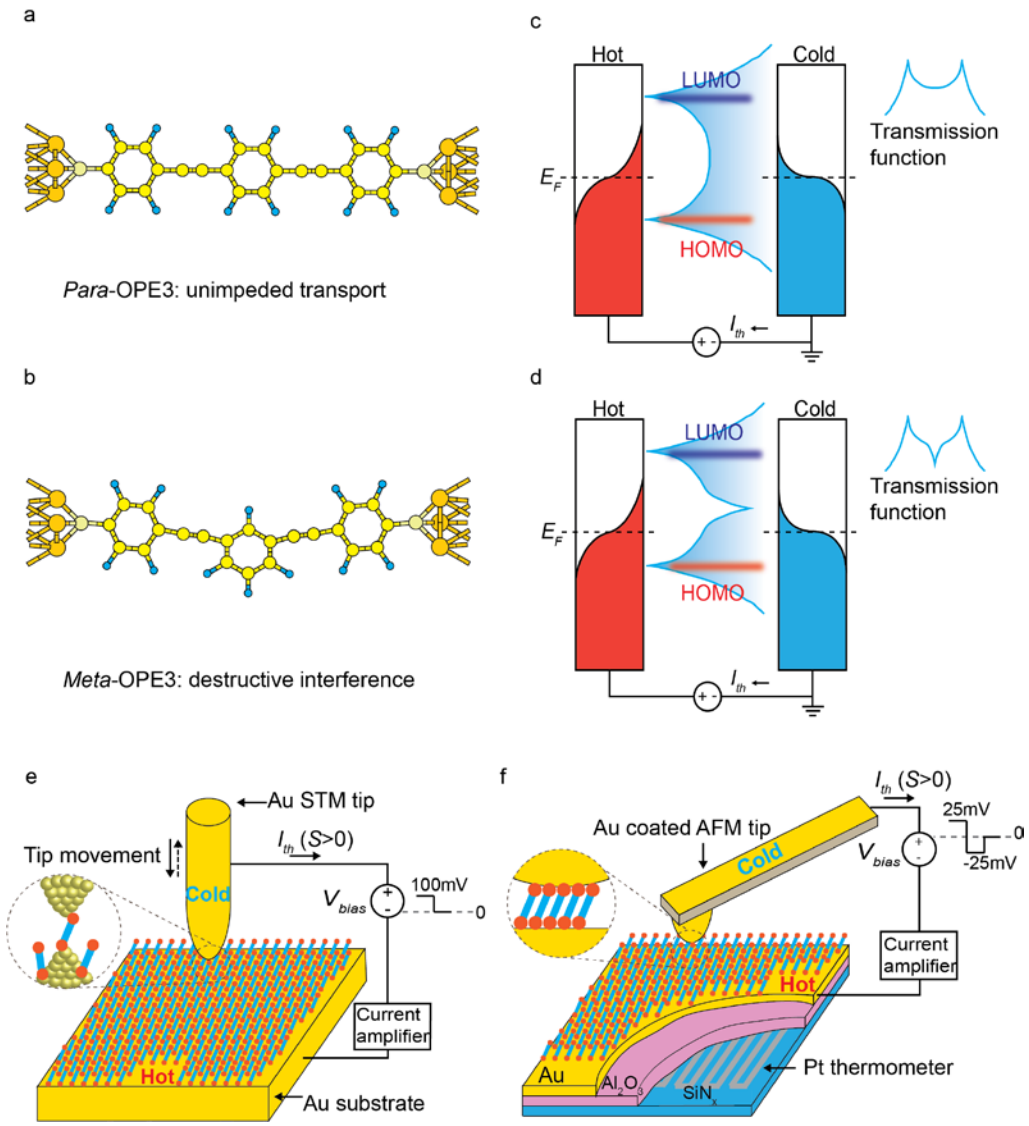

Figure 1. Schematics describing transport in molecular junctions and experimental approaches. a,b, Geometry of Au-(*para*-OPE3)-Au and Au-(*meta*-OPE3)-Au junctions, respectively. c, Schematic description of the origin of thermocurrent in a molecular junction in which charge transport is dominated by the HOMO level. The transmission function is to be a sum of two Lorentzians. d, Thermocurrent in a molecular junction with destructive interference. The transmission shows sharp features, unlike a Lorentzian-type transmission. e, Schematic of the experimental setup based on an STM break junction. Molecules are trapped between the Au STM tip and Au substrate when the tip repeatedly approaches the substrate and withdraws from it. A voltage bias is applied and the current is monitored to evaluate the conductance. In thermoelectric measurements the substrate is heated to the desired temperature and the tip is kept at ambient temperature. No voltage bias is applied to the junction and the thermocurrent is recorded to estimate the thermoelectric voltage. The inset shows the formation of a single-molecule junction. f, Schematic of the experimental setup employed for measuring the thermoelectric properties in a many-molecule junction. It is based on an AFM, where a Au-coated cantilevered probe makes contact with a molecular monolayer self-assembled on gold. The inset shows a many-molecule junction. The direction of the thermocurrent I_{th} in panels a, b corresponds to a positive sign of the Seebeck coefficient.

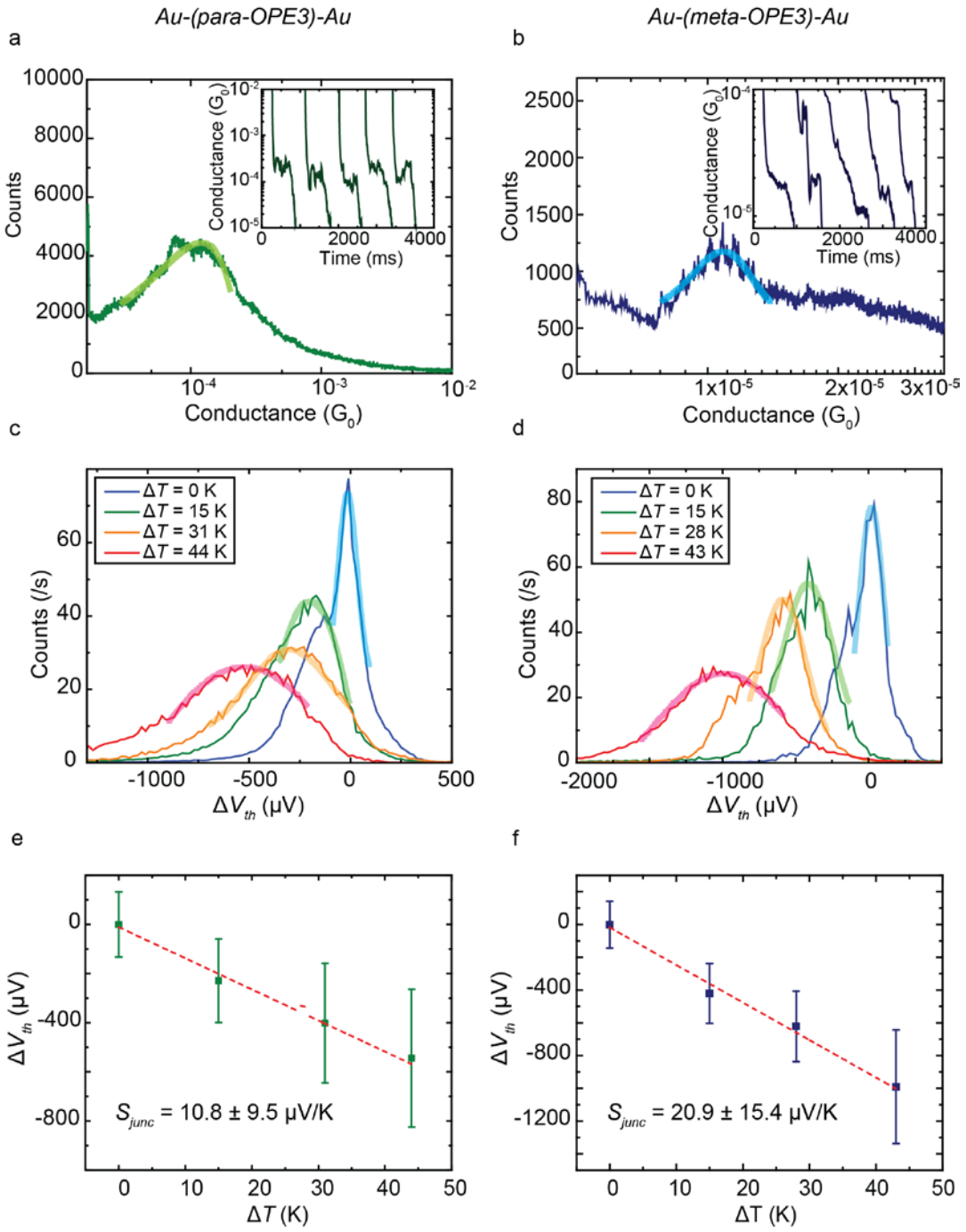

Figure 2. Results of single-molecule junction experiments with Au-(*para*-OPE3)-Au (left column) and Au-(*meta*-OPE3)-Au (right column), respectively. a,b, Conductance histograms, generated without data selection from 2000 traces. The curved lines show Gaussian fits. The insets display representative traces. c,d, Distribution of thermoelectric voltages at a series of ΔT as indicated. Shaded curves represent Gaussian fits. e,f, Thermoelectric voltage as a function of ΔT. Red dashed lines are linear fits.

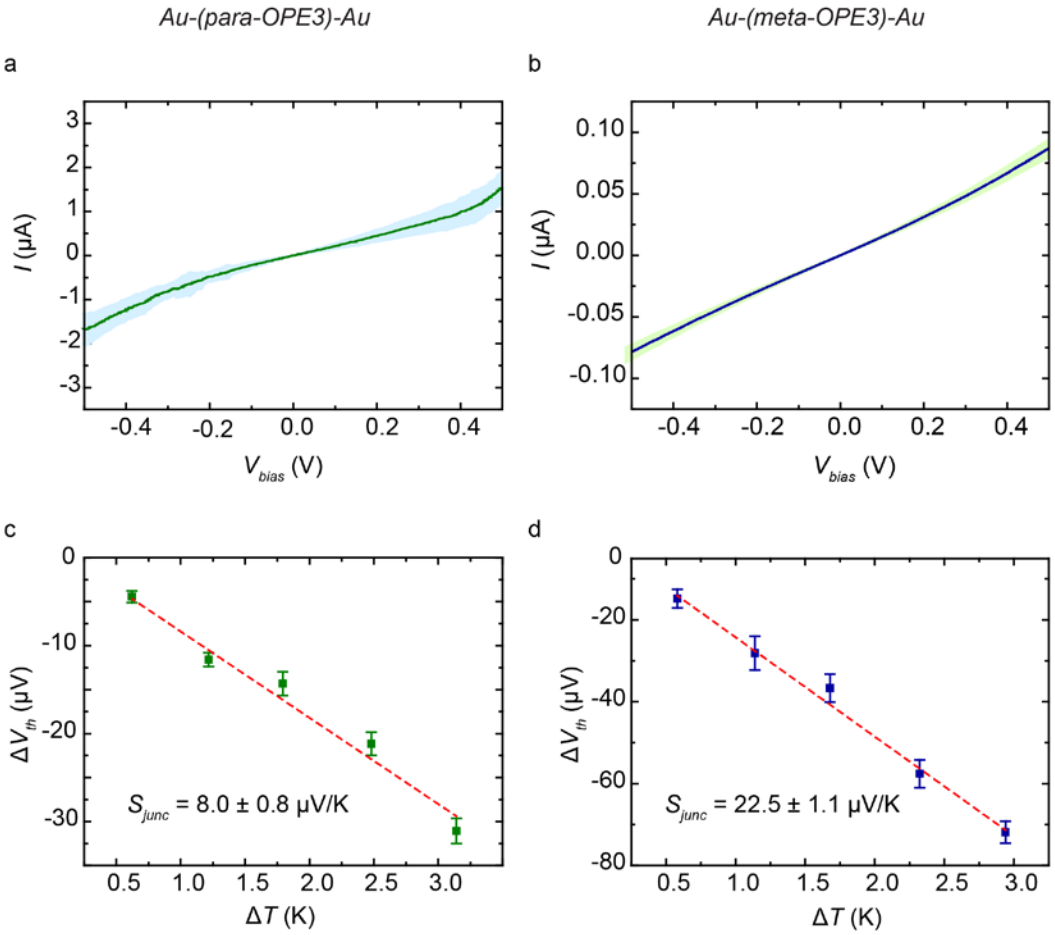

Figure 3. Results for monolayer measurements of Au-(*para*-OPE3)-Au (left column) and Au-(*meta*-OPE3)-Au junctions (right column), respectively. a,b, *I*-*V* characteristics obtained by averaging 50 individual *I*-*V* curves. The shaded regions represent the standard deviations. c,d, Thermoelectric voltage as a function of Δ*T*. Red dashed lines are linear fits.

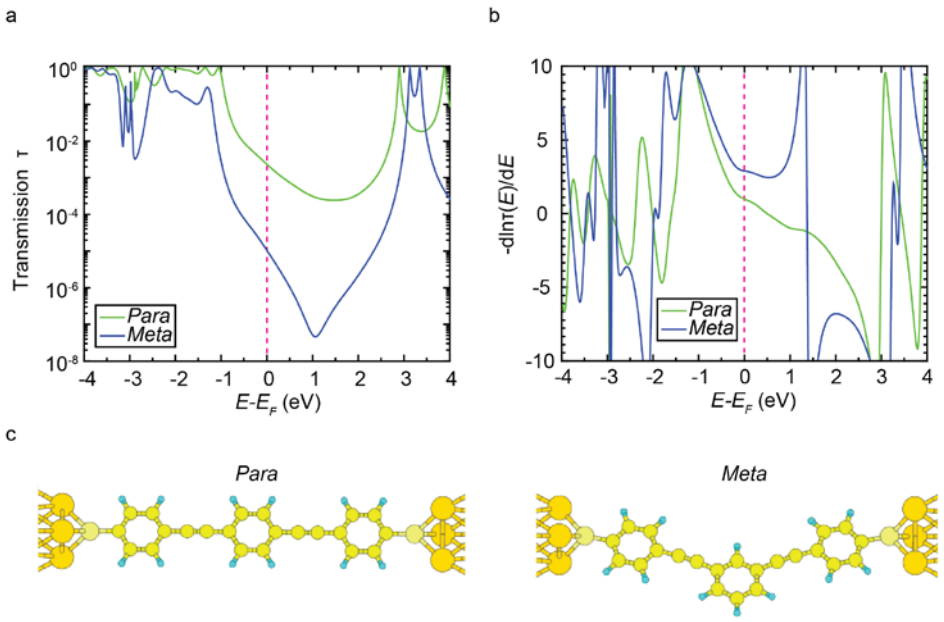

Figure 4. Theoretical computational results for Au-(*para*-OPE3)-Au and Au-(*meta*-OPE3)-Au from DFT+Σ calculations. a, Transmission curves. b, Negative derivatives of the logarithm of the transmission curves. These are proportional to the thermopower. c, The single-molecule junction geometries considered in our DFT+Σ calculations for the para and the meta molecular junctions.